arXiv:1302.0943v1 [astro-ph.SR] 5 Feb 2013

The mean-field solar dynamo with double cell meridional circulation pattern

V.V. Pipin[1−3] and A.G. Kosovichev[3]

[1]Institute of Solar-Terrestrial Physics, Russian Academy of Sciences,

[2] Institute of Geophysics and Planetary Physics, UCLA, Los Angeles, CA 90065, USA

[3]Hansen Experimental Physics Laboratory, Stanford University, Stanford, CA 94305, USA

Received ______________________; accepted ______________________

Abstract

The paper addresses the question whether the dynamo remains of the solar type if it is coupled with the two-cell in radius meridional circulation pattern. The answer is positive for a wide class of dynamo models that take into account the subsurface rotational shear. We show that the Gleisberg-type cycles, representing variations of 11-year on the centure time scale, can be generated due to a nonlinear resonance between the dynamo wave, and the large-scale magnetic field amplification in the middle of the convection zone as a result of the convergent meridional shearing flows. The conditions of such resonant interaction depends on the speed of the meridional flow and other details of the model.

Subject headings: Dynamo — Magnetohydrodynamics (MHD) — Sun:dynamo

1. Introduction

It is widely believed that the sunspot activity of the Sun is governed by the hydromagnetic turbulent dynamo operating deep in the solar convection zone. The meridional circulation, which is observed on the surface as a steady flow from the equator to the poles with a speed of 10-20 m/s, is often considered as an important ingredient of the solar dynamo (Dikpati & Charbonneau, 1999; Charbonneau, 2011). It is suggested that the return meridional flow in the deep convection zone can promote the drift of sunspot activity to the equator in the course of the 11-year solar cycle (so-called "butterfly diagram"), as well as the meridional drift of the poloidal magnetic field on the solar surface from mid-latitudes to the poles. This idea is extensively used in the Babcock-Leighton type solar dynamo models. Despite, the mean-field dynamo models may reproduce the main properties the solar cycles without the meridional circulation (e.g., Pipin & Kosovichev 2011b; Pipin 2013), the circulation affects details of the model. In particular if the dynamo effect is distributed in the bulk of the convection zone, the circulation properties affect the magnetic field distribution with depth. For example, the meridional circulation pattern, which is derived from a mean field model of the solar differential rotation has the latitudinal flow concentrated to the boundaries of the convection zone (Kitchatinov, 2011). Such circulation swaps the toroidal magnetic fields to the bottom of the convection zone, and the poloidal magnetic fields get concentrated to the pole (Pipin & Kosovichev, 2011a). The helioseismology inversions suggest that the global circulation may consist of two cells in the radial direction (see, Mitra-Kraev & Thompson 2007; Zhao et al. 2012). In the northern hemisphere, the flow direction is from the equator to the poles at the top of the convection zone, and the flow direction is reversed in the bottom cells. Such double-cell circulation is also obtained by numerical simulations (Miesch et al., 2006, 2011; Guerrero et al., 2013). The influence of multi-cell circulation on the flux-transport dynamo models was studied by Bonanno et al. (2006); Jouve & Brun (2007). They found that in case of the double-cell circulation pattern, the evolution of the large-scale toroidal and poloidal magnetic field of the Sun is qualitatively different from the observations.

In this Letter we examine effects of the double-cell meridional circulation pattern (see, Fig1c) on a mean-field dynamo model, in which the magnetic field generation is distributed in the bulk of the convection zone, and the migration of the magnetic field on the surface is controlled by the subsurface rotational shear layer action. This type of the subsurface-shear shaped dynamo was suggested by Brandenburg (2005) and was extensively studied in our recent papers (e.g., Pipin & Kosovichev 2011c). In particular, it was found that the dynamo model can reproduce the known statistical relation of the solar cycle (Pipin et al., 2012). Here, we investigate effects of the double-cell meridional circulation pattern on this model, and show that the resulted evolution of the large-scale magnetic field is in qualitative agreement with observations.

2. Dynamo equations

We consider a large-scale axisymmetric magnetic field, $\bar{\mathbf{B}}=\mathbf{e}_{\phi}B+\nabla\times\frac{A\mathbf{e}_{\phi}}{r\sin\theta}$, where $B(r,\theta,t)$ is the azimuthal component of the magnetic field, $A(r,\theta,t)$ is proportional to the azimuthal component of the vector potential, r is the radial coordinate, and θ is the polar angle. The mean flow is given by velocity vector $\overline{\mathbf{V}}=\mathbf{e}_{r}\overline{U}_{r}+\mathbf{e}_{\theta}\overline{U}_{\theta}+\mathbf{e}_{\phi}r\sin\theta\Omega$, where $\Omega\left(r,\theta\right)$ is the angular velocity of the solar differential rotation, and $\overline{U}_{r}(r,\theta)$ and $\overline{U}_{\theta}(r,\theta)$ represent velocity components of the meridional circulation. The mean magnetic field is governed by the dynamo equations:

$$\frac{\partial\overline{\mathbf{B}}}{\partial t}=\nabla\times\left(\overline{\mathbf{V}}\times\overline{\mathbf{B}}+\boldsymbol{\mathcal{E}}\right),\tag{1}$$

where mean electromotive force $\boldsymbol{\mathcal{E}}$ is given by Pipin (2008)(hereafter P08):

$$\mathcal{E}_{i}=\left(\alpha_{ij}+\gamma_{ij}^{(\Lambda)}\right)\overline{B}_{j}-\left(\eta_{ijk}+\eta_{ijk}^{(\delta)}\right)\nabla_{j}\overline{B}_{k}.\tag{2}$$

The tensor α_{ij}, representing the so-called α-effect, includes hydrodynamic ($\alpha_{ij}^{(H)}$) and magnetic ($\alpha_{ij}^{(M)}$) helicity contributions:

$$\begin{aligned}
\alpha_{ij} &= C_{\alpha}\psi_{\alpha}\sin^{2}\theta\alpha_{ij}^{(H)}+\alpha_{ij}^{(M)}, && (3)\\
\alpha_{ij}^{(H)} &= \delta_{ij}\left\{3\eta_{T}\left(f_{10}^{(a)}\left(\mathbf{e}\cdot\mathbf{\Lambda}^{(\rho)}\right)+f_{11}^{(a)}\left(\mathbf{e}\cdot\mathbf{\Lambda}^{(u)}\right)\right)\right\}+ && (4)\\
&+ e_{i}e_{j}\left\{3\eta_{T}\left(f_{5}^{(a)}\left(\mathbf{e}\cdot\mathbf{\Lambda}^{(\rho)}\right)+f_{4}^{(a)}\left(\mathbf{e}\cdot\mathbf{\Lambda}^{(u)}\right)\right)\right\}+\\
& 3\eta_{T}\left\{\left(e_{i}\Lambda_{j}^{(\rho)}+e_{j}\Lambda_{i}^{(\rho)}\right)f_{6}^{(a)}+\left(e_{i}\Lambda_{j}^{(u)}+e_{j}\Lambda_{i}^{(u)}\right)f_{8}^{(a)}\right\},
\end{aligned}$$

where $\mathbf{\Lambda}^{(\rho)}=\boldsymbol{\nabla}\log\overline{\rho}$ quantifies the density stratification, $\mathbf{\Lambda}^{(u)}=\frac{1}{2}\boldsymbol{\nabla}\log\left(\eta_{T}^{(0)}\right)$ quantifies the stratification of turbulent diffusivity $\eta_{T}^{(0)}$, and $\mathbf{e}=\mathbf{\Omega}/\left|\mathbf{\Omega}\right|$ is a unit vector along the axis of rotation. The α-quenching function $\psi_{\alpha}=-3/4\phi_{6}^{(a)}\left(\beta\right)$ depends on $\beta=\left|\overline{B}\right|/\sqrt{\overline{\rho}\mu_{0}\overline{u^{2}}}$, and $\phi_{6}^{(a)}$ is given in P08.

The turbulent pumping, $\gamma_{ij}^{(\Lambda)}$, depends on the mean density and turbulent diffusivity stratification, and also on the Coriolis number $\Omega^{*}=2\tau_{c}\Omega_{0}$, where τ_{c} is a typical convective turnover time, and Ω_{0} is the angular velocity. Following the results of P08, $\gamma_{ij}^{(\Lambda)}$ is expressed as follows:

$$\begin{aligned}
\gamma_{ij}^{(\Lambda)} &= 3\eta_{T}\left\{f_{3}^{(a)}\Lambda_{n}^{(\rho)}+f_{1}^{(a)}\left(\mathbf{e}\cdot\mathbf{\Lambda}^{(\rho)}\right)e_{n}\right\}\varepsilon_{inj}-3\eta_{T}f_{1}^{(a)}e_{j}\varepsilon_{inm}e_{n}\Lambda_{m}^{(\rho)}, && (5)\\
&- 3\eta_{T}\left(\varepsilon-1\right)\left\{f_{2}^{(a)}\Lambda_{n}^{(u)}+f_{1}^{(a)}\left(\mathbf{e}\cdot\mathbf{\Lambda}^{(u)}\right)e_{n}\right\}\varepsilon_{inj}.
\end{aligned}$$

The turbulent diffusivity is anisotropic due to the Coriolis force, and is given by:

$$\eta_{ijk}=3\eta_{T}\left\{\left(2f_{1}^{(a)}-f_{2}^{(d)}\right)\varepsilon_{ijk}-2f_{1}^{(a)}e_{i}e_{n}\varepsilon_{njk}\right\}. \tag{6}$$

We also include the nonlinear effects of magnetic field generation induced by the large-scale current and the global rotation, which are usually called as the $\Omega\times J$-effect or the δ dynamo effect (Rädler, 1969). Their importance is supported by the numerical simulations (Käpylä et al., 2008; Schrinner, 2011). We use the equation for $\eta_{ijk}^{(\delta)}$ which was suggested in P08 (also, see, Rogachevskii & Kleeorin, 2004):

$$\eta_{ijk}^{(\delta)}=3\eta_{T}C_{\delta}f_{4}^{(d)}e_{j}\left\{\tilde{\varphi}_{7}^{(w)}\delta_{ik}+\tilde{\varphi}_{2}^{(w)}\frac{\overline{B}_{i}\overline{B}_{k}}{\overline{B}^{2}}\right\}, \tag{7}$$

where, C_{δ} measures the strength of the $\Omega\times J$ effect, $\tilde{\varphi}_{2,7}^{(w)}\left(\beta\right)$ are normalized versions of the magnetic quenching functions $\varphi_{2,7}^{(w)}$ given in P08. They are defined as follows, $\tilde{\varphi}_{2,7}^{(w)}\left(\beta\right)=\frac{5}{3}\varphi_{2,7}^{(w)}\left(\beta\right)$. The functions $f_{\{1-11\}}^{(a,d)}$in Eqs(3,5,6, 7) depend on the Coriolis number. They can be found in P08, as well.

In our models we use the solar convection zone model computed by Stix (2002). The mixing-length is defined as $\ell=\alpha_{\mathrm{MLT}}\left|\Lambda^{(p)}\right|^{-1}$, where $\Lambda^{(p)}=\boldsymbol{\nabla}\log\overline{p}$ is the inverse pressure scale height, and $\alpha_{\mathrm{MLT}}=2$. The turbulent diffusivity is parameterized in the form, $\eta_{T}=C_{\eta}\eta_{T}^{(0)}$, where $\eta_{T}^{(0)}=\dfrac{u'^{2}\tau_{c}}{3f_{ov}\left(r\right)}$ is a profile of the mixing-length turbulent diffusivity, ℓ is a typical correlation length of the turbulence, C_{η} is a constant to control the efficiency of large-scale magnetic field dragging by the turbulent flow. Also, we modify the mixing-length turbulent diffusivity by factor $f_{ov}(r)=1+\exp\left(50\left(r_{ov}-r\right)\right)$, where $r_{ov}=0.725R_{\odot}$ to model saturation of the turbulent parameters near the bottom of the convection zone, as suggested by the numerical simulations (see, e.g., Ossendrijver et al. 2001, 2002; Käpylä et al. 2008). The results do not change much if we scale the turbulent diffusivity gradient $\boldsymbol{\Lambda}^{(u)}=C_{v}\boldsymbol{\nabla}\log\left(\eta_{T}^{(0)}\right)$ with a factor $C_{v}\le0.5$. For values of greater C_{v} our model leads to a steady non-oscillating dynamo which is concentrated to the bottom of the convection zone. Note, that the models by Bonanno et al. (2002); Bonanno (2012) use $C_{v}=0$. We introduce the additional parameters C_{v} and function $f_{ov}(r)$ to model the distribution of the helicity coefficient α closer to the results of the numerical simulations.

The bottom of the integration domain is at $r_{b}=0.715R_{\odot}$, and the top of the integration domain is $r_{e}=0.99R_{\odot}$. Pipin & Kosovichev (2011a) showed that the solar-type dynamo solution can be obtained for $C_{\alpha}/C_{\delta}\ge2$. In that paper we found that the approximate threshold for magnetic field generation is $C_{\alpha}\approx0.03$ for a diffusivity scaling factor $C_{\eta}=0.05$ to match the 22-year periodicity. Figure 1 shows the radial profiles for the α-effect coefficients, the isotropic and anisotropic parts of the turbulent diffusivity and the $\Omega\times J$

effect. They are in the qualitative agreement with the simulations results by Ossendrijver et al. (2001) and Käpylä et al. (2009).

The meridional flow is modeled in the form of four stationary circulation cells with two cells along the radius in each hemisphere. The pattern is modeled by the stream function Ψ, $\overline{\mathbf{U}} = \frac{U_0}{\overline{\rho}}\boldsymbol{\nabla}\times\left(\mathbf{e}_{\phi}\boldsymbol{\Psi}\right)$, where we assume the following analytic form to describe the radial and latitudinal dependence of Ψ:

$$\begin{aligned} \Psi &= \frac{2c_m}{\pi}\left(x_m^2 - x^2\right)\left(\frac{1}{x} - x_e\right)^{1.5}\sin\left(\frac{\pi\left(x - x_i\right)}{\left(x_e - x_i\right)}\right)\times \\ &\times \left(\tanh\left(20k\right)\left(x^2 - x_i^2 - 1\right) + 1\right)\left(\frac{\partial P_2}{\partial\theta} + m\frac{\partial P_4}{\partial\theta}\right), \end{aligned} \tag{8}$$

where, U_0 is the amplitude of the flow, $x = r/R$ is a distance in the units of the solar radius, $x_m = r_m/R$ is the stagnation point of the upper cell, $x_i = r_i/R$ is the inner boundary of the integration domain, $x_e = r_e/R$ is the upper boundary of the integration domain; parameter m controls the number of cells in latitude, and parameter k is to control the strength of the flow at the bottom of the convection zone; c_m is the constant to normalize the maximum of the flow amplitude to 1. In the model, we use $x_m = 0.89$, $k = 0$ and $m = -1/3$, that gives $c_m = 1/14$ for $x_i = 0.715$ and $x_e = 0.99$. The given parameters result in the circulation pattern shown in Figure 1c. This pattern resembles qualitatively the results of the helioseismology inversions (Mitra-Kraev & Thompson, 2007, also Zhao et al 2012). Note, that for $x_m = 0$ and keeping the others parameters the same we would get a single-cell (per hemisphere) flow pattern which is close to the mean-field models results (see, Kitchatinov 2011). If we additionally put $k = 1$, then the amplitude of the flow near the bottom of the convection zone is reduced strongly. For $m > 1/3$, secondary latitudinal cells become pronounced at the high latitude .

The contribution of small-scale magnetic helicity $\overline{\chi} = \overline{\mathbf{a}\cdot\mathbf{b}}$ ($\mathbf{a}$ and $\mathbf{b}$ are the fluctuating parts of magnetic field vector-potential and magnetic field vector) to the α-effect is defined as follows (P08):

$$\alpha_{ij}^{(M)} = 2f_2^{(a)}\delta_{ij}\frac{\overline{\chi}\tau_c}{\mu_0\overline{\rho}\ell^2} - 2f_1^{(a)}e_ie_j\frac{\overline{\chi}\tau_c}{\mu_0\overline{\rho}\ell^2}. \tag{9}$$

The nonlinear feedback of the large-scale magnetic field to the α-effect is described by a dynamical quenching due to the constraint of the total magnetic helicity conservation. The latter can be written as follows(Hubbard & Brandenburg, 2012; Pipin, 2013):

$$\begin{aligned}\frac{d}{dt}\int\left\{\overline{\chi}+\overline{\mathbf{A}}\cdot\overline{\mathbf{B}}\right\}dV &= -\eta\int\left\{\overline{\mathbf{B}}\cdot\overline{\mathbf{J}}+\overline{\mathbf{b}\cdot\mathbf{j}}\right\}dV \\ &\quad -\int\boldsymbol{\nabla\cdot}\boldsymbol{\mathcal{F}}^{\chi}dV\end{aligned} \tag{10}$$

where integration is performed over the volume that comprises the dynamo region, $\boldsymbol{\mathcal{F}}^{\chi}$ is the diffusive flux of the total helicity which results from the turbulent motions, η is the molecular diffusivity. The differential equation that corresponds to the Eq.(10) is:

$$\frac{\partial\overline{\chi}}{\partial t} = -\frac{\partial\left(\overline{\mathbf{A}}\cdot\overline{\mathbf{B}}\right)}{\partial t} - \frac{\overline{\chi}}{R_m\tau_c} - \eta\overline{\mathbf{B}}\cdot\overline{\mathbf{J}} - \boldsymbol{\nabla\cdot}\boldsymbol{\mathcal{F}}^{\chi} - \left(\overline{\mathbf{U}}\cdot\boldsymbol{\nabla}\right)\left(\overline{\chi}+\overline{\mathbf{A}}\cdot\overline{\mathbf{B}}\right), \tag{11}$$

where $\boldsymbol{\mathcal{F}}^{\chi} = -\eta_{\chi}\boldsymbol{\nabla}\left(\overline{\chi}+\overline{\mathbf{A}}\cdot\overline{\mathbf{B}}\right)$. We assume $R_m = 10^6$ and $\eta_{\chi} = 0.1\eta_T$. To solve Eq.(11) the large-scale vector-potential $\overline{\mathbf{A}}$ is required. For axisymmetric large-scale magnetic fields the vector-potential can be represented as a sum of the azimuthal and poloidal components (Krause & Rädler, 1980):

$$\overline{\mathbf{A}} = \mathbf{e}_{\phi}T + \mathbf{r}P = \frac{\mathbf{e}_{\phi}}{r\sin\theta}A + r\mathbf{e}_rP. \tag{12}$$

The toroidal part of the vector potential is governed by the dynamo equations (Eq.1). The poloidal part of the vector potential can be restored from the toroidal magnetic field component using equation $\boldsymbol{\nabla}\times(\mathbf{r}P) = \mathbf{e}_{\phi}B$. The reconstruction is simple for the pseudo-spectral numerical schemes which are based on the Legendre polynomial decomposition for the latitude profile of the large-scale toroidal field. We matched the dynamo solution to the potential field model outside the convection zone, and assume the perfect conductivity condition at the bottom boundary. For the magnetic helicity we employ $\bar{\chi} = 0$ at the bottom of the convection zone and we assume that the the radial derivative of the total helicity is zero at the top. The initial magnetic field is assumed dipolar with a small quadrupolar component to check the parity preference when the solution reach the steady state.

3. Results and discussion

Figure 2 shows the snapshots of the magnetic field evolution in the North segment of the solar convection zone for the models without and with the meridional circulation. We observe drift of the dynamo waves related to the evolution of the large-scale toroidal and poloidal fields, towards the equator and towards the pole, respectively. It is found that circulation accelerates the equator-ward drift of the toroidal magnetic field near the surface and the poleward drift of the toroidal magnetic field the near bottom of the convection zone. The strength of the radial magnetic field at the poles is increased as well. It is also found that the double-cell circulation reduce the toroidal magnetic field strength inside the convection zone. This effect is generally expected for the circulation-dominated flux-transport dynamo models, for which an increase of the circulation speed increases the dynamo generation threshold in terms of the α-effect coefficient. This, in turn, decreases of the period of the dynamo cycle.

The time-latitude “butterfly” diagrams of the toroidal magnetic field evolution in the upper part of the solar convection zone and the similar diagrams for the radial magnetic field at the surface are shown in Figure 3. In all cases (with and without circulation) there is the qualitative agreement with observations. We found that the maximum of the toroidal magnetic field migrates closer to the equator for the models with $U_0 = 10$ and $U_0 = 15$ m/s. However, in these cases the butterfly diagram wings are wider in latitude than in the case

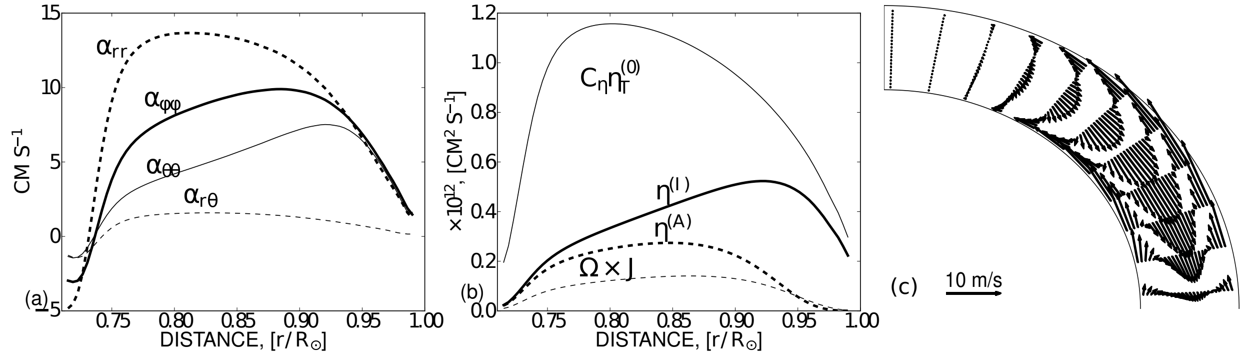

Fig. 1.— Panel (a), the radial profiles of components of the helicity coefficient α (Eq.3) for $\theta = 45^\circ$; panel (b), the radial profiles of the background turbulent diffusivity $C_\eta \eta_T^{(0)}$, the isotropic, $\eta^{(I)}$, and anisotropic, $\eta^{(A)}$, parts of the magnetic diffusivity coefficient, and the $\Omega \times J$ term (Eq. 7); (c), velocity vectors of the double-cell meridional circulation pattern .

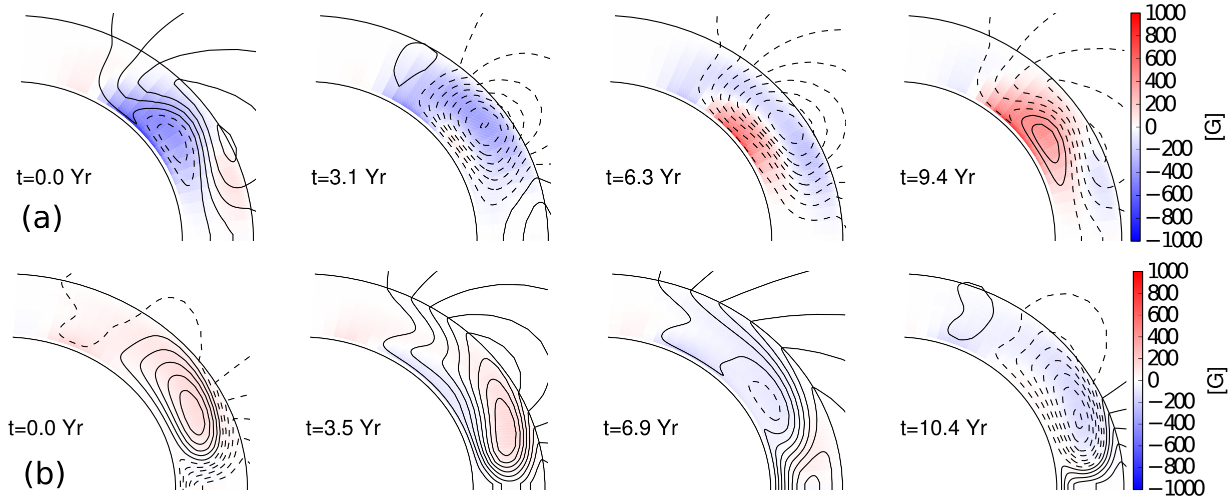

Fig. 2.— Snapshots of the magnetic field evolution inside the North segment of the convection zone for the dynamo model: (a) shows the model without meridional circulation; (b), the model with the meridional circulation with the maximum speed $U_0 = 10$ m/s. The field lines show of the poloidal component of the mean magnetic field, and the toroidal magnetic field (varies ±1kG) is shown by gray scale background images.

without circulation. Also it is found that the circulation reduces the latitudinal width of the polar branch for the radial magnetic field evolution and also reduces the overlap between the cycles. We draw these diagrams only for one hemisphere because in all these cases the antisymmetric mode (dipolar) is dominant.

However, the changes of the dynamo properties with increase of U_0 from 0 to 15 m/s are not monotonic. We found a resonance-like phenomenon for the model with the flow speed $U_0 = 5$ m/s. For this case, the evolution of the magnetic fields shows long-term periodic variations, which correspond to a torus-like attractor on the dynamo phase diagram (see, e.g., Knobloch et al. 1998). In this case, the short-term (11-year) cycles are modulated by a grand cycle with a period of 80-90 years, corresponding to the so-called "Gleisberg" cycle. Figure 4 shows some results for the model with $U_0 = 5$ m/s. We found that the Gleisberg cycle appears irrespective of the magnetic helicity feedback (Eq. 11). The only difference is that for the model without the magnetic helicity feedback, the long-term variations keep the dipole-like symmetry relative to the equator. In the model with the magnetic helicity feedback, the maximum of the magnetic activity periodically drifts from one hemisphere to another on the long time scale. Figure 4 shows the simulated sunspot number (defined by Pipin et al. 2012) and the polar flux variations. The polar flux is defined as the total $\overline{B}_r$ above $\pm 60^\circ$ latitude. The model shows that the polar flux reversal time can be different in the two hemispheres. The similar effect was reported earlier by Pipin (1999) for the nonlinear model that included a nonlinear feedback of magnetic field on the angular momentum balance in the solar convection zone. Figure 4(c) shows that the average polar flux in the northern hemisphere is larger than in the southern one. This is because of the asymmetric initial conditions and due to the parity conservation in the model.

We can interpret the obtained long-term variations as a nonlinear resonance between the dynamo wave propagation and the increase of the magnetic field in the middle of the

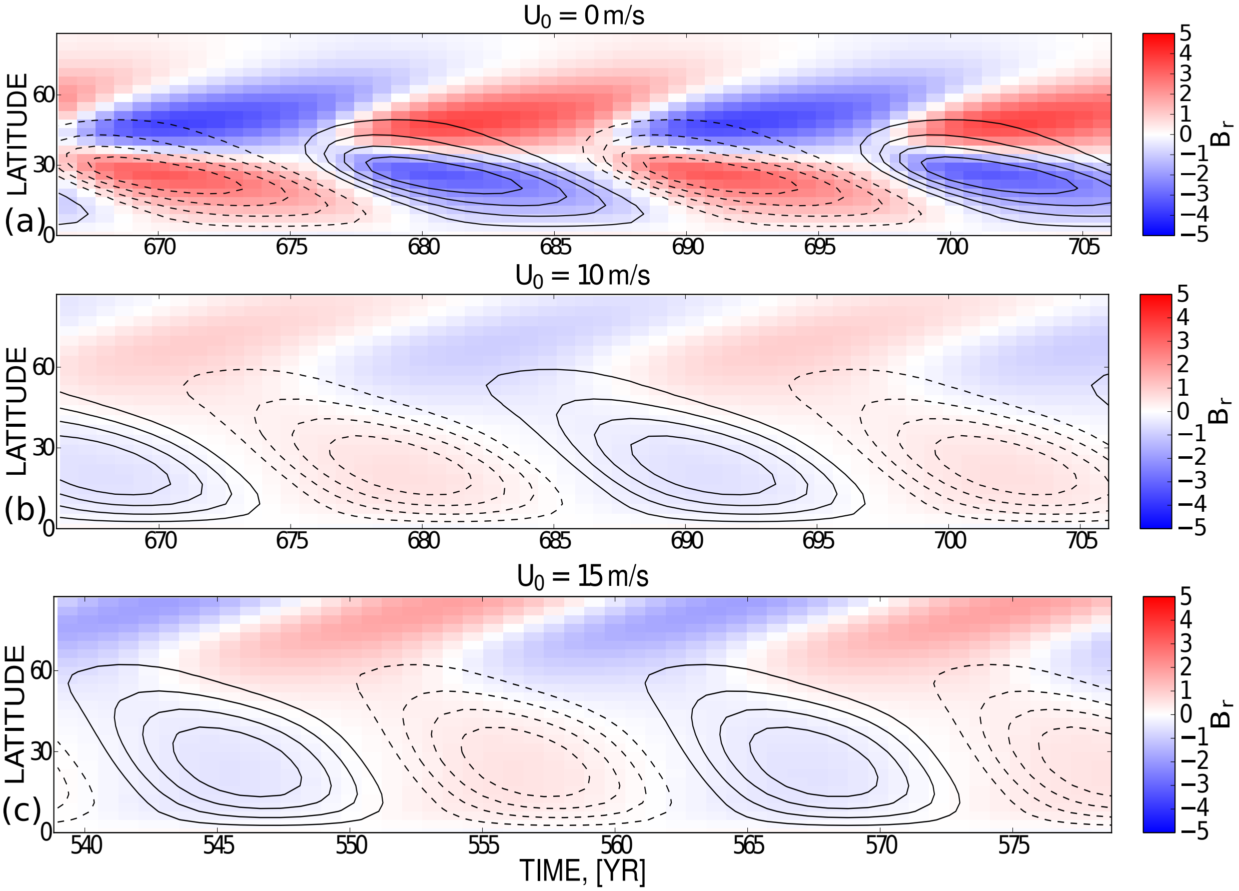

Fig. 3.— (a) the time - latitude variations ("butterfly diagrams") for the model without meridional circulation; (b) the same for the model with the meridional circulation with the maximum speed $U_0 = 10$ m/s; (c) the same as (b) for the $U_0 = 15$ m/s. The toroidal field near the surface, at $r = 0.95R_{\odot}$, is shown by contours (plotted for ±100G range) and the radial magnetic field at the surface is shown background images.

convection zone due to the convergence of meridional flows from the top and bottom of the convection zone. The long-term modulation (Gleisberg cycle) disappears if we discard the nonlinear part of the δ effect ($\Omega \times J$ term in Eq.7). Note that in Eq.(7) the function $\tilde{\varphi}_7^{(w)}(\beta)$ is monotonically quenched to zero when the magnetic field equipartition parameter β is growing. Function $\tilde{\varphi}_2^{(w)}(\beta)$ is non-monotonic, and has a maximum at $\beta \approx 1$. Moreover, the structure of the second term in Eq.(7) is the same as for the helicity coefficient α effect because the associated electromotive force is proportional to $\frac{3}{2}\eta_T C_\delta f_4^{(d)} \tilde{\varphi}_2^{(w)} \overline{B}_i \left(\mathbf{e}\cdot\boldsymbol{\nabla}\right) \log \overline{\mathbf{B}}^2$ (see details in P08 and also in Rogachevskii & Kleeorin 2004). Our interpretation for the origin of the long-term modulation is supported by the fact that for the given dynamo number C_α the long-term oscillations are excited only within a narrow range of the circulation amplitude, e.g., for $C_\alpha = 0.025$, the resonance circulation speed is $U_0 \approx 5$ m/s. The long-term periodicity disappears for $U_0 \approx 3$ m/s and $U_0 = 7$ m/s. Moreover, for the $U_0 = 10$ m/s the similar long-term periodicity is excited for $C_\alpha = 0.035$. We guess that the similar resonance could exist for the mean-field dynamo with double cell meridional circulation and the α effect due to buoyancy instability (see, e.g., Chatterjee et al., 2011), because the latter is proportional to $\nabla \bar{B}^2$ as the nonlinear part of the δ effect.

For the excitation of the North-South asymmetric grand cycle the effect of the magnetic helicity is important. The growth rate of the quadrupolar modes is smaller than for the dipolar ones. This leads to the quenching of the asymmetric perturbations. The nonlinear feedback of the magnetic helicity on the magnetic field generation results in the time-delay of the α-effect quenching. When the typical time-delay become comparable with the growth time of the grand cycle the asymmetric perturbations leads to excitation of the long-term asymmetric cycles. The nonlinear time-delay feedback on the magnetic field generation is usually considered as important mechanism of the grand cycles excitation (Yoshimura, 1978; Kichatinov et al., 1994; Covas et al., 1998; Knobloch et al., 1998; Pipin, 1999).

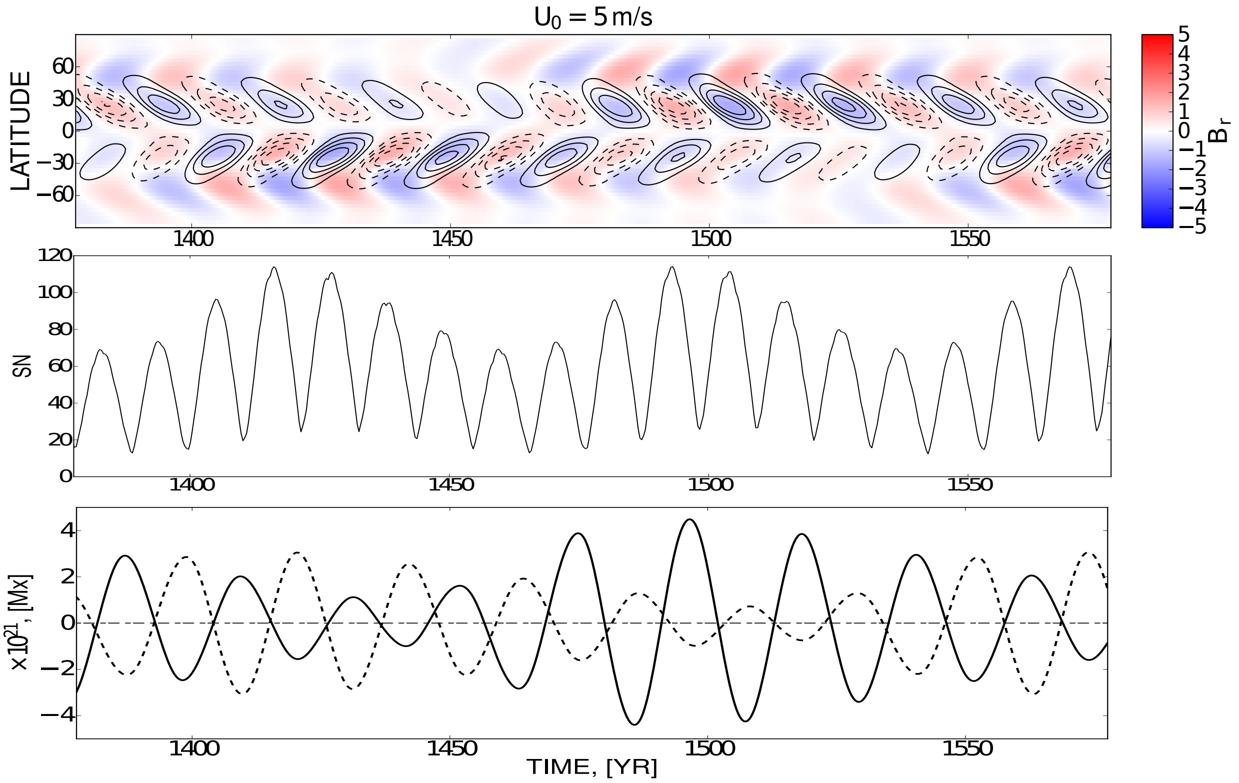

Fig. 4.— Panel (a) toroidal (contours) and radial (background images) fields for the speed $U_0 = 5$ m/s; panel (b) shows the simulated sunspot number (SN) as a function of time (see, Pipin et al. 2012); (c) the corresponding polar flux in the northern (solid) and southern (dashed) hemispheres.

We investigated the stability of the obtained solutions with respect to changes of the circulation pattern and the other parameters of the model. In addition to the previous discussion, we found that the long-term modulation disappears when we neglect the convective overshooting effect, i.e., when we put $f_{ov}(r) = 1$. The results similar shown in Figures 2(b) and 3(b,c), are obtained for the case of pure a $\alpha^2\Omega$ dynamo (without the $\Omega \times J$ effect). However, in this case, the cycle overlap in the time-latitude diagrams is much stronger than in Figures 3(b,c). The similar time-latitude butterfly-diagrams are obtained also for the case when the meridional circulation forms only one cell per hemisphere with the stagnation point radius larger than $0.85R$. This is because of the subsurface rotational shear layer included in the model. For the deeper stagnation point the dynamo wave is dominated by the toroidal magnetic field near the bottom of the convection zone (Pipin & Kosovichev, 2011a). Also, we checked the effect of the meridional circulation in the simplified model which was presented by Pipin & Kosovichev (2011c). In that model the α-effect was confined in the low-latitude $\pm 30^{\circ}$ zone. The results are generally similar to what is shown in Figures 2(b) and 3(b,c).

The main findings can be summarized as follows. The mean-field dynamo model that includes the subsurface rotational shear layer and the double-cell (in radius) meridional circulation, indicated by the recent helioseismology results, can reproduce the solar magnetic cycles in the form of the time-latitude “butterfly” diagrams. The double-cell circulation affects the distribution of the magnetic field with radius in the convection zone, increasing the field concentration to the convection zone boundaries, and to the layer of the two cells convergence in the middle of the convection zone. The latter effect can lead to a result in a nonlinear resonance between the dynamo wave accompanied by large-scale magnetic field amplification in the middle of the convection zone as the result of the convergent flows. The resonance conditions depend on the flow speed and other details of the model. This resonance leads to a long-term modulation of the dynamo cycles, resembling the Gleisberg

100-year solar cycles. In this case the solution can be North-South asymmetric due to unstable quadrupole component.

REFERENCES

Bonanno, A. 2012, Geophys. Astrophys. Fluid Dyn., 1

Bonanno, A., Elstner, D., Belvedere, G., & Rüdiger, G. 2006, Memorie della Societa Astronomica Italiana Supplementi, 9, 71

Bonanno, A., Elstner, D., Rüdiger, G., & Belvedere, G. 2002, A&A, 390, 673

Brandenburg, A. 2005, ApJ, 625, 539

Charbonneau, P. 2011, Living Reviews in Solar Physics, 2, 2

Chatterjee, P., Mitra, D., Rheinhardt, M., & Brandenburg, A. 2011, A&A, 534, A46

Covas, E., Tavakol, R., Tworkowski, A., & Brandenburg, A. 1998, A&A, 329, 350

Dikpati, M., & Charbonneau, P. 1999, ApJ, 518, 508

Guerrero, G., Smolarkiewicz, P. K., Kosovichev, A., & Mansour, N. 2013, in Solar and Astrophysical Dynamos and Magnetic Activity, IAUS 294

Hubbard, A., & Brandenburg, A. 2012, ApJ, 748, 51

Jouve, L., & Brun, A. S. 2007, A&A, 474, 239

Käpylä, P. J., Korpi, M. J., & Brandenburg, A. 2008, A&A, 491, 353

—. 2009, A&A, 500, 633

Kichatinov, L. L., Rüdiger, G., & Kueker, M. 1994, Astron. Astrophys., 292, 125

Kitchatinov, L. L. 2011, in Astronomical Society of India Conference Series, Vol. 2, Astronomical Society of India Conference Series, 71–80

Knobloch, E., Tobias, S. M., & Weiss, N. O. 1998, MNRAS, 297, 1123

Krause, F., & Rädler, K.-H. 1980, Mean-Field Magnetohydrodynamics and Dynamo Theory (Berlin: Akademie-Verlag), 271

Miesch, M. S., Brown, B. P., Browning, M. K., Brun, A. S., & Toomre, J. 2011, in IAU Symposium, Vol. 271, IAU Symposium, ed. N. H. Brummell, A. S. Brun, M. S. Miesch, & Y. Ponty, 261–269

Miesch, M. S., Brun, A. S., & Toomre, J. 2006, ApJ, 641, 618

Mitra-Kraev, U., & Thompson, M. J. 2007, Astronomische Nachrichten, 328, 1009

Ossendrijver, M., Stix, M., & Brandenburg, A. 2001, A&A, 376, 713

Ossendrijver, M., Stix, M., Brandenburg, A., & Rüdiger, G. 2002, A&A, 394, 735

Pipin, V. V. 1999, A&A, 346, 295

—. 2008, Geophysical and Astrophysical Fluid Dynamics, 102, 21

Pipin, V. V. 2013, in Solar and Astrophysical Dynamos and Magnetic Activity Proceedings IAU Symposium No. 294

Pipin, V. V., & Kosovichev, A. G. 2011a, ApJ, 738, 104

—. 2011b, ApJ, 741, 1

—. 2011c, ApJL, 727, L45

Pipin, V. V., Sokoloff, D. D., & Usoskin, I. G. 2012, A&A, 542, A26

Rädler, K.-H. 1969, Monats. Dt. Akad. Wiss., 11, 194

Rogachevskii, I., & Kleeorin, N. 2004, ArXiv Astrophysics e-prints

Schrinner, M. 2011, A&A, 533, A108

Stix, M. 2002, The sun: an introduction, 2nd edn. (Berlin : Springer), 521

Yoshimura, H. 1978, ApJ, 226, 706

Zhao, J., Bogart, R. S., Kosovichev, A. G., & Duvall, Jr., T. L. 2012, in American Astronomical Society Meeting Abstracts, Vol. 220, American Astronomical Society Meeting Abstracts #220, 109.05

This manuscript was prepared with the AAS LaTeX macros v5.2.